

Magnetic phospholipid tubes connected to magnetoliposomes: Pearling instability induced by a magnetic field

C. Ménager^{1,a}, M. Meyer¹, V. Cabuil¹, A. Cebers², J.-C. Bacri³, and R. Perzynski³

¹ Laboratoire LI2C, Equipe Colloïdes Inorganiques, Université Pierre et Marie Curie, Case 63, UMR 7612, 4 place Jussieu, 75252 Paris Cedex 05, France

² Institute of Physics, University of Latvia, Salaspils-1, LV-2169, Latvia

³ Laboratoire LMDH, Université Pierre et Marie Curie, Université Denis Diderot, Case 78, 4 place Jussieu, 75252 Paris Cedex 05, France

Received 6 April 2001 and Received in final form 14 March 2002

Abstract. We propose here a method to modify the membrane tension of phospholipid tubes with an applied magnetic field. The tubes are connected to giant liposomes capping the tubes at both ends. Tubes and liposomes are all filled with a magnetic fluid. The tension of the tube membrane is tuned by the deformation of the ending liposomes under the applied field. We modelize the magnetoliposome deformation and we are then able to describe the tube evolution. At low magnetic fields, the tube remains at equilibrium with a cylindrical shape and a uniform radius. It responds to an increase of membrane tension by a diameter reduction. Above a magnetic-field threshold, the cylindrical shape becomes unstable with respect to a pearling deformation. The tube shape then selected by the system is an unduloid, with a constant mean curvature equal to C_0 , the spontaneous curvature of the membrane.

PACS. 82.70.Dd Colloids – 75.50.Mm Magnetic liquids – 87.16.Dg Membranes, bilayers, and vesicles

Lipid bilayers in water form not only quasi-spherical vesicles, but also tubular closed membranes that have attracted recently the attention of biophysicists. Very long cylindrical vesicles are found in the Golgi apparatus and may play an important role in the cellular traffic [1,2]. Morphological instabilities of membranes in a cylindrical geometry are different from those of spherical vesicles and may lead to original phenomena. An example of such an instability is produced on radial tubular protusions of adhesive cells by the disruption of their actin cytoskeleton [3]. This gradual disruption induces the transformation of the cylindrical cell extensions into a periodic chain of pearls. The so-called “pearling” instability is a general phenomenon of flexible tubes under tension and has been found some time ago in the case of phospholipid bilayers [4–6]. Bar-Ziv describes a pearling instability induced by the application of laser tweezers on long cylindrical lipid vesicles. The origin of this Rayleigh-like instability has been identified as a competition between the external tension induced by the laser and the bending rigidity of the membrane. In the case of biological cells it is the rigidity of the actin shell that balances the tension produced by adhesion points. Similar phenomena have also been observed in nerve fibers when they are subjected to a stretch or when the cytoskeleton is disrupted [7,8].

Another example is the coiling conformation induced in multilamellar tubes made of stacked bilayers doped with anchored polymers [9,10] or the pearling instabilities observed on hollow tubular lipid vesicles due to hydrophilic polymer with hydrophobic side groups [11]. But in these two cases the pearling instability is caused by a polymer adsorption which induces a spontaneous curvature of the membrane, it is not a tension-induced pearling instability as in [3–6]. For flexible tubes made of a single bilayer, a peristaltic undulation is observed sometimes at the onset of the pearling instability. In [12] pearling is described as a preliminary stage in the budding instability when the quasi-spherical shape of a liposome is disrupted by a sudden increase of the osmotic pressure.

In the present work we describe a pearling instability induced when a magnetic field is applied on phospholipid tubular vesicles (tubes) filled with a magnetic fluid [13]. These tubes consist in long and thin cylinders of membrane anchored at both ends to large spheres (liposomes), which gives them the overall shape of dumbbells. The originality of this system is that the stress is not exerted on the tube itself, but on the liposomes connected to it. Under a magnetic field of low intensity (300 Oe), the magnetoliposomes at the tube ends elongate along the field direction. The tension increases both in the spherical and in the cylindrical parts as it is uniform all along the fluid mem-

^a e-mail: menager@ccr.jussieu.fr

brane. The tube develops a pearling instability in order to relax this excess of surface tension. Another outstanding point is that the liposomes and the tube can exchange a membrane area.

1 Experiments

1.1 Materials

– The *magnetic fluid* (or ferrofluid) is a colloidal dispersion of maghemite ($\gamma\text{-Fe}_2\text{O}_3$) nanoparticles dispersed in water at $\text{pH } 7$ [14]. The magnetic particles have a diameter of the order of 10 nm. They are negatively charged and are indeed stabilized by electrostatic repulsion between grains. The negative surface charges are due to ionized citrate ligands. A residual ionic strength is due to unadsorbed citrate species in equilibrium with the adsorbed ones $[\text{Na}_3\text{Cit}] = 0.28 \text{ mol L}^{-1}$. The volume fraction of magnetic oxide before encapsulation is 6%.

– The *phospholipid* constituting the membrane is 1-2 dioleoyl-sn-glycero-3-phosphocholine (DOPC, Sigma). Its phase transition temperature (T_c) is -22°C so that the phospholipid molecules are always in the fluid-like state at room temperature. Even though phosphocholine is neutral (with a zwitterionic head), a weak negative surface charge due to impurities has been evidenced [15,16]. There is indeed no affinity between the negatively charged particles and the negative membrane.

1.2 Preparation of phospholipid tubes

The preparation of phospholipid tubes has been described succinctly in the literature [3,17]. Tubes are always obtained from the hydration of a phospholipid film under an induced flow of water. In [4,5], they are anchored at both ends to lipid globules. In our case the system is noticeably different because tubes are anchored not to lipid globules but to giant liposomes exhibiting thermal fluctuations visible by optical microscopy. The method we use to encapsulate the ferrofluid inside the tube has already been described to prepare magnetic liposomes [18]: 0.5 mg of DOPC as a dry powder is mixed with $5 \mu\text{L}$ of the aqueous dispersion of magnetic nanoparticles and sheared on a cover slide of optical microscopy with a glove finger. The oily orange film then obtained is presumably a lamellar phase swelled with magnetic particles. Immediately following the shearing, $50 \mu\text{L}$ of tridistilled water is poured onto the film to start the spontaneous swelling. The water is added directly in the observation cell consisting in two cover slides separated by a paraffin-based spacer (Parafilm, American National Can, melt on a hot stage and squeezed between the two slides). The thickness of the cell is of the order of $200 \mu\text{m}$. Tubes form quickly and can be observed fifteen minutes after the beginning of hydration.

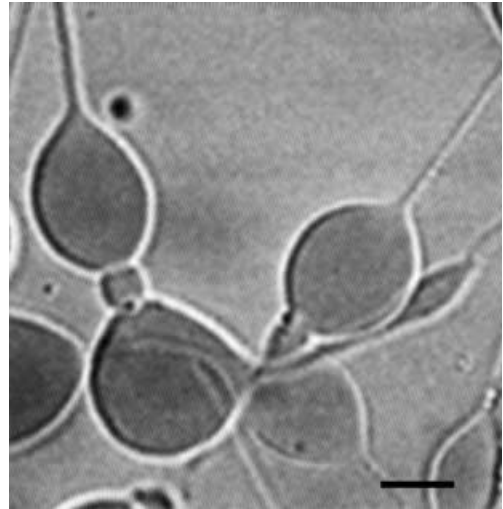


Fig. 1. Phospholipid tubes and liposomes as observed by optical microscopy. Tubes and liposomes are linked together, the magnetic fluid is inside the structures and can be easily localized due to its contrast. The membrane exhibits large thermal fluctuations. The bar length is $20 \mu\text{m}$.

1.3 Experimental methods

Due to the orange color of the encapsulated ferrofluid, the samples can be observed by *optical microscopy* (Leica 40x, NA 0.65). The volume fraction of magnetic particles encapsulated inside the magnetoliposomes is of the order of 0.002% or 10^{14} particles/ cm^3 estimated from the color observed and from previous magneto-phoresis experiments [18]. The sample is placed between two pairs of coils (500 turns each) oriented at 90° allowing to control the direction of the applied magnetic field. The magnetic-field intensity can be adjusted between 15 and 310 Oe. The magnetic field is applied gradually by steps of 15 Oe each 30 seconds. The pictures recorded with a CCD camera are digitized with a frame grabber (LG-3, Scion Corp. Frederick, MD USA).

Transmission Electron Microscopy (TEM) is performed using a JEOL 100CXII top entry UHR. The samples are deposited on a carbon film and negatively stained with ammonium molybdate.

2 Experimental observations

2.1 Without magnetic field

Optical microscopy: A sample prepared as described above exhibits a lot of tubes and liposomes which are linked together (Fig. 1). Tubes and liposomes are stable (over many hours) and thermal fluctuations are visible. The radius R_{ves}^0 of the liposomes ranges from 30 to $80 \mu\text{m}$ (see Tab. 1). They are quasi-spherical or pear-like shaped. Most of them are connected to very long cylindrical structures of length larger than $500 \mu\text{m}$. The circular section of these tubes has a radius R_0 which varies between 1.25 to $2.5 \mu\text{m}$ (see

Table 1. Physical characteristics of the magnetoliposome samples. R_{ves}^0 : initial radius of the magnetoliposome —optically determined. R_0 : initial radius of the phospholipid tube connected to the magnetoliposome —optically determined. H_{pearling} : magnetic field at which the first non-uniform deformations of the tube are transiently observed. $\tau_0 = \frac{K_b}{2R_0^2}$: tension of the liposome membrane in zero field —deduced from R_0 with $K_b = 21kT$. A and H^* : parameters of equation (12) deduced from plots $Y = f(X^{0.25}/H)$ as presented in Figure 8. $\frac{S_{\text{tube}}^0}{S_{\text{ves}}^0}$: ratio of the initial surface of the half-tube to that of the magnetoliposome. It is deduced from A and K_b values using equation (11): $\frac{S_{\text{tube}}^0}{S_{\text{ves}}^0} = \frac{A}{336\pi}$. L : half-length of the tube deduced from $\frac{S_{\text{tube}}^0}{S_{\text{ves}}^0}$, R_0 and R_{ves}^0 : $L = \frac{2(R_{\text{ves}}^0)^2}{R_0} \frac{S_{\text{tube}}^0}{S_{\text{ves}}^0} \cdot \frac{\Delta S^{\text{pearling}}}{S_{\text{ves}}^0}$. Ratio evaluated by $\frac{A}{336\pi} \left(1 - \frac{R_{\text{pearling}}}{R_0}\right) \approx 0.4 \frac{A}{336\pi}$. $\frac{\Delta V^{\text{pearling}}}{V_{\text{ves}}^0}$: ratio evaluated by $\frac{3R_0 A}{2R_{\text{ves}}^0 336\pi} \left(1 - \left(\frac{R_{\text{pearling}}}{R_0}\right)^2\right) \approx 0.96 \frac{R_0 A}{R_{\text{ves}}^0 336\pi}$. C_0 : spontaneous curvature deduced in the pearling regime from Figure 9b using equations (A.4) and (16).

Vesicle sample	R_{ves} (μm)	R_0 (μm)	H_{pearling} (kA/m)	τ_0 (10^{-8} J m^{-2})	H^* (kA/m)	A
A	27.8	1.3	4.95	2.5	0.95	470
B	36.6	2.5	3.38	0.67	0.66	549
C	51	1.6	4.74	1.7	0.55	362
D	54.6	2.1	6.18	0.93	1.30	253
E	55.1	1.25	3.71	2.7	0.64	296
F	58.3	2.4	5.05	0.75	0.84	371
G	66.6	1.7	2.47	1.5	0.98	210
H	73.4	1.65	4.94	1.5	0.76	142
I	77.5	1.45	6.18	2	0.74	162

Vesicle sample	$S_{\text{tube}}^0/S_{\text{ves}}^0$	L (mm)	$\frac{\Delta S^{\text{pearling}}}{S_{\text{ves}}^0}$	$\frac{\Delta V^{\text{pearling}}}{V_{\text{ves}}^0}$	Field direction with respect to the tube	C_0 (μm^{-1})
A	0.44 ₅	0.53	18 %	2 %	\perp	/
B	0.52	0.56	21 %	3.4 %	//	/
C	0.34 ₅	1.14	14 %	1 %	\perp	0.033 ₂
D	0.24	0.67	10%	0.9 %	//	0.029 ₆
E	0.28	1.37	11 %	0.6 %	\perp	0.030 ₁
F	0.35	1.01	14 %	1.4 %	\perp	0.029 ₁
G	0.20	1.06	8 %	0.5 %	\perp	0.023 ₇
H	0.13 ₅	0.88	5 %	0.3 %	\perp	0.021 ₄
I	0.15 ₅	1.29	6 %	0.3 %	//	0.020 ₄

Tab. 1). All the experiments are here performed in a simple configuration. The selected systems are always constituted of two liposomes connected at each extremity of a tube and not connected with any other tube or liposome (Figs. 2a and 3).

TEM: (Fig. 4) Even though the phospholipid membrane is a bit disrupted by the staining technique, the electron microscopy pictures show nanoparticles confined inside the lumen of the cylinders. The tube in Figure 4 has a diameter of 0.2 μm , which is much smaller than the diameter in solution because of the drying process and the staining technique. Its length is much larger than the field of view.

2.2 Application of a magnetic field

When a magnetic field is applied to an isolated liposome, the thermal fluctuations of its membrane progressively

vanish and the liposome elongates along the field [19]. By comparison the elongation is much larger for a liposome connected to a tube (Fig. 2b). The deformation under a magnetic field is characterized by assimilating the elongated liposome to a prolate ellipsoid of the following parameters: a semi-axis along the field, b semi-axis normal to the field and eccentricity $e = \sqrt{1 - \frac{b^2}{a^2}}$. Liposomes connected to a tube reach significantly higher eccentricities (for example, $e = 0.97$ for $H = 220$ Oe) than isolated liposomes ($e = 0.63$ for the same value of H). If the magnetic-field intensity is large enough, a sinusoidal instability develops, leading to a peristaltic modulation of the tube diameter with a finite amplitude (Fig. 5). We note for each magnetoliposome the magnetic field H_{pearling} associated to the first observation of a precursor peristaltic modulation of the tube (see Tab. 1). We call it hereafter the “transient onset of pearling” as the peristaltic modulation frequently disappears in a few seconds, the tube reaching

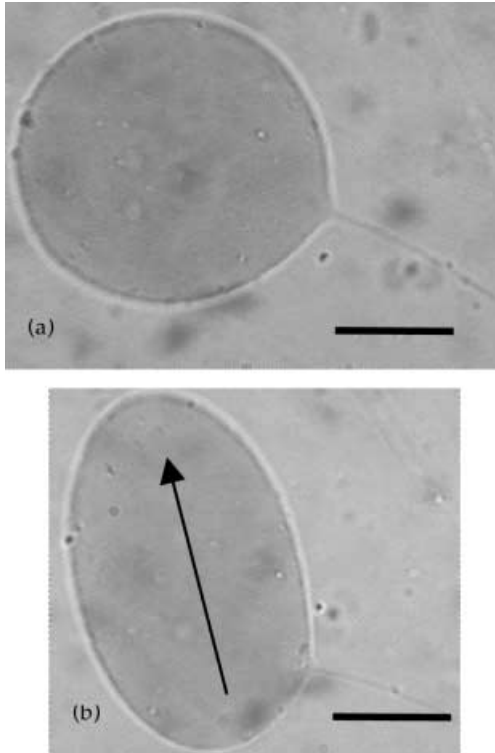


Fig. 2. A magnetoliposome connected to one tube (a) without magnetic field, the shape is almost like a sphere of radius R_{ves}^0 ; (b) under a magnetic field (here 24 kA/m, direction given by the arrow), the liposome elongates along the field direction. The diameter of the tube is close to the optical microscopy resolution; however, one can see that its radius decreases during the deformation. The bar length is 20 μm .

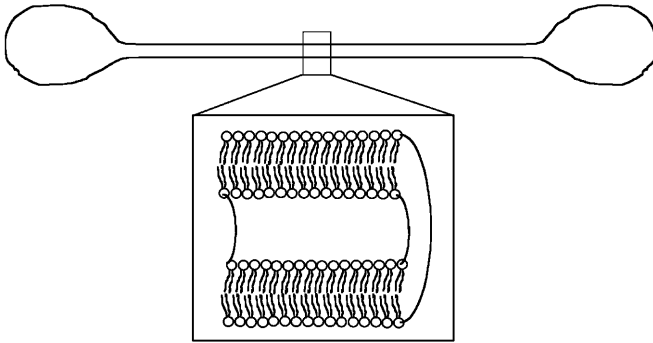


Fig. 3. Schema of the system chosen for the deformation study. The liposome is connected to one tube with a continuous membrane which is the same for the tube and for the liposome. The phospholipid used here is DOPC. The magnetic fluid is encapsulated inside the system.

then its equilibrium radius under the applied field. We call “pearling regime” the field domain $H > H_{\text{pearling}}$. The experimental wavelength λ between the pearls is of the order of 10 to 30 μm , but its measure is biased by the fact that the pearls often travel along the tube.

An important feature of this instability is that it is independent of the orientation of the magnetic field with respect to the tube axis.

3 Theoretical description

The deformation of quasi-spherical magnetoliposomes (*not connected to a tube*) into prolate ellipsoids when a magnetic field is applied, can be explained by the flattening of thermal undulations due to the magnetic stress [19]. Briefly, the deformation is measured as a function of the field intensity and plotted as e^4 vs. $\ln(H^2)$. The limiting slope in high fields leads to the bending modulus K_b of the bilayer, firstly introduced by Helfrich [20,21].

The bending modulus K_b deduced for those liposomes encapsulating a ferrofluid has the same value (of the order of 10^{-19}J) as other measurements with non-magnetic liposomes made of the same lipid. To explain here the larger deformation under field of magnetoliposomes connected to one tube, we propose the following scenario: under the field the two magnetoliposomes at the tube ends increase the membrane tension. The new equilibrium shape corresponds to a tube of lower radius, while the liposomes at the ends absorb the equivalent amount of lipids coming from the tube. For a large tension of the membrane the pearling instability is observed. This instability is equivalent to the classical Rayleigh instability of a liquid cylinder under surface tension [22]. As the membrane tension is related to the elongation of the two capping liposomes, we use their deformation under field to understand how the lipid tubes filled with a magnetic fluid evolve.

3.1 Isolated liposomes

We first recall here the basis of the model describing the deformations of isolated magnetoliposomes submitted to a magnetic field [19]. The formalism of [19] ($e \ll 1$) is here extended to ellipsoids of any elongation. It is well established that an increase of the surface tension τ of a closed membrane induces an unfolding of its thermal undulations and, equivalently, an increase of the projected surface area S_τ . We note, respectively, S_{τ_0} and τ_0 the initial values of surface area and tension for the strongly fluctuating liposome in zero magnetic field. The deformation of a giant liposome due to tension follows a relation of elasticity that is particular to its entropic nature [23]:

$$\frac{(S_\tau - S_{\tau_0})}{S_{\tau_0}} \cong \frac{kT}{8\pi K_b} \ln \left(\frac{\tau}{\tau_0} \right). \quad (1)$$

We assimilate the elongated liposome to an ellipsoid of eccentricity e and of constant volume. For small deformations, the projected area reduces to

$$S_\tau \cong S_{\tau_0} \left(1 + 2\frac{e^4}{45} \right). \quad (2)$$

If a magnetic field H is applied, its intensity is related to the tension τ of the membrane. Because of the magnetic discontinuity at the boundary of the magnetoliposome, between the inside and the outside media, a magnetic force (per unit area) develops: $2\pi (\vec{M}\vec{n})^2 \vec{n}$, \vec{M} being the magnetization of the magnetic liquid induced inside the vesicle

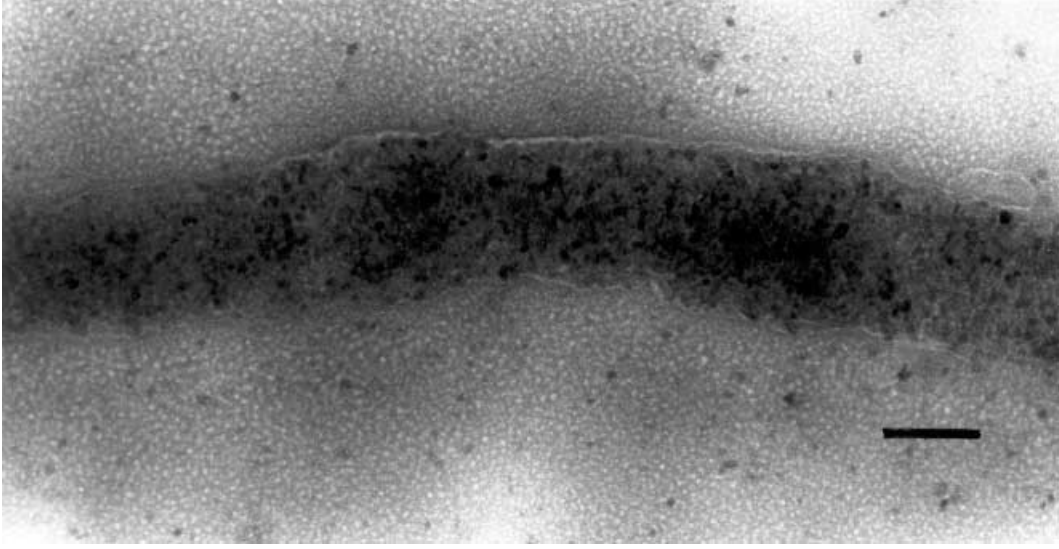


Fig. 4. Transmission electron microscopy of a negatively stained sample (ammonium molybdate). Even if the membrane is a bit disrupted by the coloration technique, magnetic particles (10 nm in diameter) are localized inside the tube. The tube diameter is around $0.2 \mu\text{m}$ (much smaller than in solution). The tube length cannot be determined by this technique. The bar length is $0.1 \mu\text{m}$.

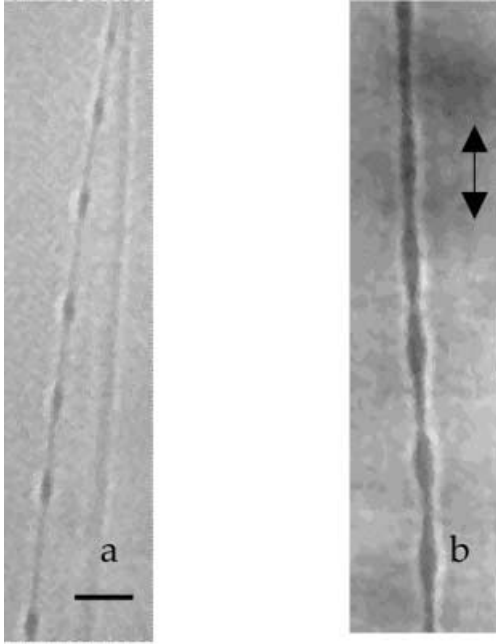


Fig. 5. Observation of the pearling instability of a tube under an applied magnetic field (its direction is along the arrow). (a) Largely developed pearling instability. The pearls travel along the tube so it can be difficult to determine a wavelength between the pearls. (b) Precursory pearling deformations, transiently observed.

by the applied field, \vec{n} being the external unit vector, normal to the surface of the vesicle. The magnetoliposome elongates along the field, exactly as a buoyant ferrofluid droplet does [24]. Assuming that the susceptibility of the magnetic fluid is low ($\mu - 1 \ll 1$, μ being the magnetic

permeability of the magnetoliposome) the magnetization is independent of the elongation and writes: $\vec{M} = \frac{(\mu-1)}{4\pi} \vec{H}$.

The balance of the forces acting on the membrane writes:

$$p_{\text{in}} - p_{\text{out}} = -2\tau\mathbf{H} + K_{\text{b}}(2\mathbf{H} + C_0)(2\mathbf{H}^2 - 2\mathbf{k}_{\text{G}} - C_0\mathbf{H}) + 2K_{\text{b}}\Delta_{\text{B}}\mathbf{H} - 2\pi(\vec{M}\vec{n})^2, \quad (3)$$

where $-\mathbf{H}$ is the mean curvature, \mathbf{k}_{G} the Gaussian curvature, C_0 the spontaneous curvature, Δ_{B} the Laplace-Beltrami operator on the surface defined as in [25,26]. Neglecting the term in curvature elasticity in comparison with the first term on the right side of relation (3), assuming an ellipsoidal shape for the vesicle and satisfying the equilibrium conditions by the virial technique, we obtain, in the limit of small deformations, the two following relations for the ellipsoidal eccentricity [24,27–29]:

$$e^2 = \frac{(\mu - 1)^2}{16\pi} \frac{H^2 R_{\text{ves}}^0}{\tau}, \quad (4)$$

and for the balance of pressures between inside (pressure p_{in}) and outside (pressure p_{out}) [30]:

$$p_{\text{in}} - p_{\text{out}} = \frac{2\tau}{R_{\text{ves}}^0} \left(1 - \frac{e^2}{3}\right). \quad (5)$$

Introducing (as in [19], with $\mu+2 \approx 3$), the reduced parameter $H^{*2} = \sqrt{\frac{45kT}{32\pi K_{\text{b}}}} \frac{16\pi}{(\mu-1)^2} \frac{\tau_0}{R_{\text{ves}}^0}$, which is homogeneous to a magnetic field, equation (4) simplifies

$$e^4 = \frac{45kT}{32\pi K_{\text{b}}} \left(\frac{\tau_0}{\tau}\right)^2 \left(\frac{H}{H^*}\right)^4. \quad (6)$$

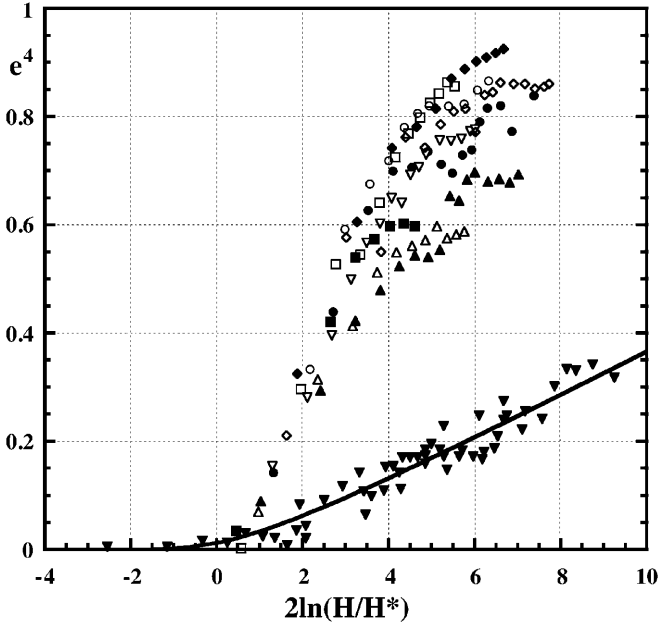


Fig. 6. Plot of e^4 as a function of $2\ln(H/H^*)$ for isolated liposomes (∇ data from Ref. [19]) and for tube-connected liposomes (\square sample A; \blacklozenge sample B; \diamond sample C; ∇ sample D; \bullet sample E; \circ sample F; \blacksquare sample G; \triangle sample H; \blacktriangle sample I —see Table 1 for the sample characteristics and the direction of the applied field). The full line is the theoretical prediction of [19] for an isolated liposome (here Eq. (8) with $\Delta S = 0$ and $e \ll 1$).

H^* is a parameter independent of H and e . It only depends on the physical characteristics of the magnetoliposome namely R_{ves}^0 , μ , K_b and its initial tension τ_0 . Figure 6 recalls the results obtained in reference [19] for isolated liposomes. Those results were all in the limit of small deformations for which $e \ll 1$. They all plot on a single master curve e^4 versus $\ln(H/H^*)^2$. The asymptotic slope at large field is proportional to the bending modulus K_b , which is found for DOPC equal to $21 \pm 2 kT$. This experimental value demonstrates that the magnetic fluid does not modify the membrane elasticity.

3.2 Under-field deformation of a magnetoliposome connected to a tube

Figure 6 compares the results obtained for isolated magnetoliposomes to the ones obtained with magnetoliposomes connected to a tube. Note that e^4 is independent of the direction of the field with respect to the one of the tube. It is clear from Figure 6 that the magnetoliposomes connected together by a tube exhibit a much stronger response to the field than isolated ones. Their deformation cannot be described anymore in the limit $e \ll 1$. Appendix A develops the formalism of Section 3.1 in the general case of any e .

In order to describe the under-field deformation of magnetoliposomes connected to a tube, we have to take

in account that the number of lipids in the overall dumbbell shape is constant. However, unlike isolated liposomes, the surface area of liposomes connected by a tube can now vary, using the cylindrical part as a reservoir of membrane. It is indeed necessary to add a supplementary term in equation (1) equal to the relative variation of surface of the liposome $\frac{\Delta S}{4\pi(R_{\text{ves}}^0)^2}$, ΔS being the excess of membrane coming from the tube in order to increase the surface of the liposome. If $\frac{\Delta S}{4\pi(R_{\text{ves}}^0)^2} \ll 1$, equation (1) then rewrites, using equation (A.2) of Appendix A,

$$f(e) - 1 = \frac{kT}{8\pi K_b} \ln \frac{\tau}{\tau_0} + \frac{\Delta S}{4\pi(R_{\text{ves}}^0)^2}. \quad (7)$$

If the ratio τ/τ_0 is now eliminated using relation (A.6), neglecting at the first order the influence of the tube on the vesicle shape, relation (7) becomes

$$\frac{16\pi K_b}{kT} (f(e) - 1) + \ln \left(\frac{8\pi K_b}{45kT} g^2(e) \right) = 4 \ln \left(\frac{H}{H^*} \right) + \frac{\Delta S}{4\pi R_{\text{ves}}^2} \frac{16\pi K_b}{kT}. \quad (8)$$

We pose

$$X = \frac{8\pi K_b}{45kT} g^2(e) = \left(\frac{\tau}{\tau_0} \right)^{-2} \left(\frac{H}{H^*} \right)^4 \quad (9)$$

(this parameter X is inversely proportional to the square of the tension induced by the field on the vesicle) and

$$Y = \frac{16\pi K_b}{kT} (f(e) - 1) + \ln X - 4 \ln H = -4 \ln H^* + \frac{\Delta S}{4\pi(R_{\text{ves}}^0)^2} \frac{16\pi K_b}{kT} \quad (10)$$

(this parameter Y is a linear function of the surface ΔS of membrane which is transferred from the tube to the liposome).

Both parameters X and Y can be calculated with equations (9) and (10) from e and H experimental values, assuming for K_b its experimental value determined in [19]. For an *isolated liposome*, $\Delta S = 0$ and $Y = -4 \ln H^*$.

The experimentally determined quantity Y is then indeed linearly related to the surface variation ΔS coming from the tube. This latter can be easily evaluated under the assumption that the increase of surface is related to a decrease of the tube radius R , assuming that the tube length L is constant (we shall see further on that this hypothesis is well founded —see Sect. 4.5 and App. C). Then the excess of the surface ΔS can be expressed as

$$\begin{aligned} \Delta S &= -2\pi L \Delta R_{\text{tube}} = 2\pi L R_0 \left(1 - \frac{R}{R_0} \right) \\ &= S_{\text{tube}}^0 \left(1 - \frac{R}{R_0} \right), \end{aligned}$$

where R_0 and R are, respectively, the tube radius in zero magnetic field and under field, L is the half-length of

the tube (each tube being connected to two magnetoliposomes), $S_{\text{tube}}^0 = 2\pi LR_0$ is the initial surface of the half-tube. Last term of expression (8) then reduces to

$$\frac{16\pi K_b}{kT} \frac{\Delta S}{4\pi (R_{\text{ves}}^0)^2} = A \left(1 - \frac{R}{R_0}\right)$$

with $A = \frac{S_{\text{tube}}^0}{S_{\text{ves}}^0} \frac{16\pi K_b}{kT}$, (11)

where $S_{\text{ves}}^0 = 4\pi (R_{\text{ves}}^0)^2$. Equation (8) then rewrites as

$$Y = -4 \ln H^* + A \left(1 - \frac{R}{R_0}\right). \quad (12)$$

3.3 Mechanical equilibrium of the cylindric tube with a uniform circular section

For a cylindric tube with a uniform circular section, the Gaussian curvature k_G and $\Delta_B \mathbf{H}$ are null. Then it comes from equation (3) with $\mathbf{H} = -\frac{1}{2R}$ that the mechanical equilibrium of the tube results, at first order, from the balance between the term of tension of the membrane and the one of bending elasticity:

$$\frac{\tau}{R} = \frac{K_b}{2R^3} (1 - C_0^2 R^2) \approx \frac{K_b}{2R^3}. \quad (13)$$

- We here assume that $p_{\text{in}} - p_{\text{out}} \ll \frac{\tau}{R}$ and $\frac{1}{2} K_b C_0^2 \ll \tau$. Those two approximations will be justified further on in Section 4.2.
- The magnetic term $2\pi (\vec{M}\vec{n})^2$, which for the vesicles is of the same order as $\frac{2\tau}{R_{\text{ves}}^0}$, can be here completely forgotten with respect to Laplace's pressure of the tube $\frac{\tau}{R}$ which is much larger than $\frac{2\tau}{R_{\text{ves}}^0}$ as $R \ll R_{\text{ves}}^0$.

In that framework, and as the K_b value is known from [19], the experimental determination of R_0 , the tube radius in zero field, allows the determination of the tension τ_0 in zero field (see Tab. 1). Typically, we find for $R_0 = 2 \mu\text{m}$, $\tau_0 = \frac{K_b}{2R_0^2} \approx 10^{-8} \text{Jm}^{-2}$.

The radius of the cylindric tube at the equilibrium is then related to the membrane tension by

$$R = \sqrt{\frac{K_b}{2\tau}}. \quad (14)$$

3.4 Onset of pearling

For high enough applied fields, a pearling transition of the phospholipid tube, analogous to the Rayleigh instability of a liquid cylinder under surface tension, can be observed. The instability here results from the competition between the *tension of the tube membrane* induced by the deformation of the ending liposomes, and the *bending modulus of the phospholipid bilayer*. In references [4–6, 31] the threshold of this pearling transition is modeled. It is given by

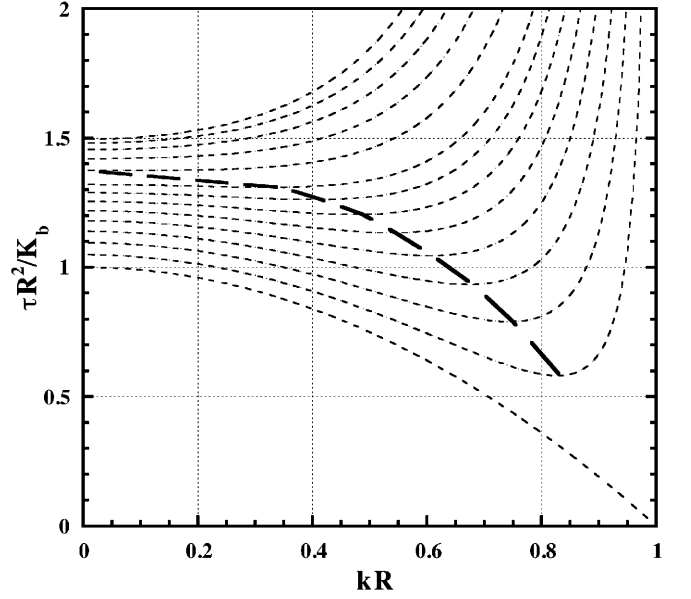


Fig. 7. Theoretical pearling threshold. Plot of $\frac{\tau R^2}{K_b}$ as a function of kR . *Thin dashed curves*: equation (15) for various values of the parameter RC_0 (from top to bottom $RC_0 = 0.1; 0.2; 0.3; 0.4; 0.5; 0.6; 0.65; 0.7; 0.75; 0.8; 0.85; 0.9; 0.95; 1$). *Thick dashed curve*: location of the minimum of the previous curves. For $RC_0 \leq 0.5$, this minimum corresponds to $kR = 0$ and $1.36 \leq \frac{\tau R^2}{K_b} \leq 1.5$.

a minimization of the parameter $\frac{\tau R^2}{K_b}$ as a function of the wave vector k , given by the following expression which depends on the spontaneous curvature C_0 :

$$\frac{\tau R^2}{K_b} + \frac{(C_0 R)^2}{2} = \frac{\frac{3}{2} - \frac{(kR)^2}{2} + (kR)^4 - 2C_0 R (kR)^2}{1 - (kR)^2}. \quad (15)$$

Figure 7 plots the variations of $\frac{\tau R^2}{K_b}$ as a function of kR for various $C_0 R$. If $C_0 R \leq 0.5$, the instability is predicted to occur at $k = 0$ (with an infinite wavelength) and for $1.36 \leq \frac{\tau R^2}{K_b} \leq 1.5$. For larger $C_0 R$ values, the instability may develop at a finite wavelength and at lower values of $\frac{\tau R^2}{K_b}$. Beyond the static analysis, a finite wavelength can also develop for kinetics reasons determined by the hydrodynamic processes inside the tube with a varying radius.

3.5 Unduloid

The shape assumed by the tube after the onset of pearling should be still a solution of the general Helfrich variation problem (Eq. (3) *without* the magnetic term which drops down for the tube). Delaunay's surfaces [32] which have a constant mean curvature, are solutions of this problem [33]. In particular, an unduloid is a Delaunay's surface with a constant mean curvature related to the spontaneous

curvature by $H = -\frac{C_0}{2}$. Equation (3) then simplifies in

$$\frac{(p_{\text{in}} - p_{\text{out}})}{\tau} = C_0. \quad (16)$$

The shape of the unduloid presents a peristaltic deformation and it could be here the shape selected by the system in the “pearling regime”. Note that the shape, selected among the family of unduloids, can be determined by a rather complex hydrodynamical process —see Section 4.4, reference [31] and references therein.

4 Experimental results and discussion

4.1 Determination of the experimental parameters A and H^* for each magnetoliposome

If the tube is a cylinder of uniform circular section, the ratio $\frac{R}{R_0}$ is, after equation (14), equal to $\sqrt{\frac{\tau_0}{\tau}}$ and thus, after equation (9), equal to $H^* \frac{X^{0.25}}{H}$. The cylindrical tube being at equilibrium, a plot of the two experimental quantities $Y = -4 \ln H^* + A \left(1 - \frac{R}{R_0}\right) = -4 \ln H^* + A \left(1 - H^* \frac{X^{0.25}}{H}\right)$ versus $\frac{X^{0.25}}{H}$ is linear with a slope $-AH^*$ and an ordinate at $\frac{X^{0.25}}{H} = 0$ equal to $Y_0 = A - 4 \ln H^*$ (see Eq. (12)). A deviation from such a linear behavior would mark that the evolution of the tube is out of the mechanical equilibrium of the cylindrical shape with a uniform circular section.

Two examples of experimental variations are presented in Figure 8 which plots Y as a function of $\frac{X^{0.25}}{H}$ for two different magnetoliposomes, each one being connected to a tube. Note that Y and $\frac{X^{0.25}}{H}$ are pure experimental parameters, fully determined by the field dependence of e for a liposome connected to one tube and by the $\frac{K_p}{kT}$ value determined with isolated liposomes [19]. As the magnetic field increases the tension increases, thus $\frac{X^{0.25}}{H}$ decreases as Y increases, meaning that ΔS the surface of membrane transferred from the tube to the vesicle increases as the field increases (at least up to the onset of pearling). It corresponds to an increase of the projected area of the magnetoliposome due to the excess of membrane coming from the tube. It is well described by the model proposed above as, until the experimental transient onset of pearling, the experimental values follow a linear behavior of negative slope. For some magnetoliposomes this linear behaviour is preserved after the transient onset of pearling, for some others a deviation is observed (see Fig. 8).

From the experimental linear behaviour of Y versus $\frac{X^{0.25}}{H}$, it is possible to determine $Y_0 = A - 4 \ln H^*$ and the slope $-AH^*$. This then allows to get for each experiment the two quantities H^* and A .

- The parameter H^* varies from 7 to 16 Oe as for isolated magnetoliposomes.
- The parameter A varies from 150 for the largest magnetoliposomes up to 550 for the smallest, meaning after equation (11) that the associated variation of the ratio $\frac{S_{\text{tube}}^0}{S_{\text{ves}}^0}$ ranges from 13% up to 52%.

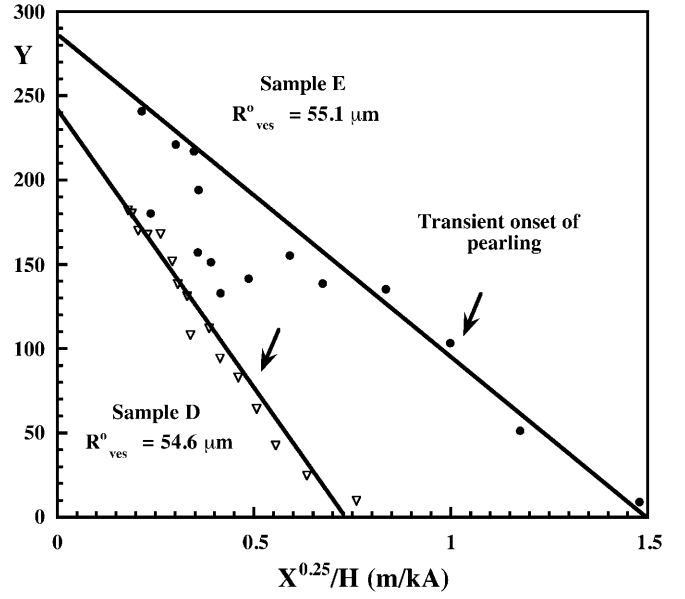


Fig. 8. Plot of Y as a function of $X^{0.25}/H$ for two liposomes connected to a tube (same symbols as in Fig. 6). The full lines are associated to the under-field equilibrium evolution of the tube with a uniform radius as given by equations (9,12) and (14). The two arrows point the experimental transient onset of pearling for the two systems (see text and Fig. 5b).

We can then deduce for each magnetoliposome:

- the half-length L of the tube, which varies from 500 μm up to 1400 μm (see Tab. 1), those variations are fully compatible with the direct optical observation;
- the reduced quantities $\frac{R}{R_0} = 1 - \frac{Y + 4 \ln H^*}{A}$ and $\sqrt{\frac{\tau_0}{\tau}} = \frac{H^*}{H} X^{0.25}$ for each applied field, and in particular their experimental values at the transient onset of pearling; whatever the initial vesicle radius, this onset corresponds to $\frac{R}{R_0} \approx \sqrt{\frac{\tau_0}{\tau}} \approx 0.6 \pm 0.1$.

Using the obtained values for $\frac{R}{R_0}$ and $\frac{S_{\text{tube}}^0}{S_{\text{ves}}^0}$, it is possible, from expression (11), to deduce for each measurement (e, H) $\frac{\Delta S}{S_{\text{ves}}^0} = \frac{S_{\text{tube}}^0}{S_{\text{ves}}^0} \left(1 - \frac{R}{R_0}\right)$, the ratio of the excess of membrane surface coming from the tube to the initial surface of the magnetoliposome. It is also possible to calculate the variation of volume $\frac{\Delta V}{V_{\text{ves}}^0} = \frac{3R_0}{2R_{\text{ves}}^0} \frac{S_{\text{tube}}^0}{S_{\text{ves}}^0} \left(1 - \left(\frac{R}{R_0}\right)^2\right)$, ΔV being the variation of volume of the magnetoliposome. The table gives an evaluation of the values of $\frac{\Delta S}{S_{\text{ves}}^0}$ and $\frac{\Delta V_{\text{tube}}}{V_{\text{ves}}^0}$ at the pearling threshold. From Table 1, it is clear that the hypothesis of constant volume (see Eqs. (A.2), (A.3), (A.4), (A.5)) for the magnetoliposome during the experiment is valid. In the whole experiment $\frac{\Delta V}{V_{\text{ves}}^0}$ remains always smaller than 5%. It confirms that the transfer of liquid from the tube to the magnetoliposome can be neglected.

On the contrary, the variation of surface of the magnetoliposome can become large. If in the whole experiment $\frac{\Delta S}{S_{\text{ves}}^0}$ is always smaller than 1, it can reach a value of 40%

in large fields for the smallest vesicles. The transfer of membrane from the tube to the magnetoliposome is thus significant. In the following we let aside the two smallest vesicles (samples A and B) for which $\frac{\Delta S_{S_0}^{\text{pearling}}}{S_0} \geq 15\%$ (see Tab. 1). Hereafter we analyze separately the experiments performed with $R_{\text{ves}} > 40 \mu\text{m}$ for which the hypothesis $\frac{\Delta S}{S_0} \ll 1$ (see Eq. (7)) can be considered as valid.

For each experiment the direction of the applied field with respect to the tube is quoted in Table 1. We are not able to point out any correlation between that direction and our experimental results. It confirms that we can neglect the magnetic term in equation (3) for the tube.

4.2 Balance of pressures: Determination of the spontaneous curvature C_0

Let us now look to the evolution of the balance of pressures $p_{\text{in}} - p_{\text{out}}$ all along the transformation. We assume that the balance is the same for the magnetoliposome and for the tube to which it is connected. We deduce $p_{\text{in}} - p_{\text{out}}$ from the magnetoliposome deformation under field using equation (A.4). Figure 9a) is a plot of $f(e) - \frac{N(e)g(e)}{2} = \frac{R_{\text{ves}}^0 (p_{\text{in}} - p_{\text{out}})}{2\tau}$ as a function of the applied field H . For $H < H_{\text{pearling}}$, $\frac{R_{\text{ves}}^0 (p_{\text{in}} - p_{\text{out}})}{2}$ is a decreasing function of H . As long as the tube evolves with an equilibrium cylindrical shape, its radius R decreases (it is a linear decreasing function of Y —see Eq. (12)) and the ratio $\frac{(p_{\text{in}} - p_{\text{out}})}{\tau}$ decreases as well. As soon as pearls begin to appear, the ratio $\frac{(p_{\text{in}} - p_{\text{out}})}{\tau}$ stops to decrease. Figure 9b) plots $\frac{(p_{\text{in}} - p_{\text{out}})}{\tau}$ in the “pearling regime” ($H > H_{\text{pearling}}$) for the magnetoliposomes of $R_{\text{ves}}^0 > 40 \mu\text{m}$. We find that this ratio is a constant (almost independent of H) as for an unduloid with a spontaneous curvature $C_0 = \frac{(p_{\text{in}} - p_{\text{out}})}{\tau}$, according to equation (16) and references [32,33]. The unduloid thus appears as the shape selected by the tube in the “pearling regime”. Moreover, the determination of $\frac{(p_{\text{in}} - p_{\text{out}})}{\tau}$ is a direct measurement of the spontaneous curvature C_0 of the liposome membrane. For $77.5 \mu\text{m} \geq R_{\text{ves}}^0 \geq 51 \mu\text{m}$, we find $2 \cdot 10^{-2} \mu\text{m}^{-1} \leq C_0 \leq 3 \cdot 10^{-2} \mu\text{m}^{-1}$ (see Fig. 9 and Tab. 1). Note that a dependence on R_{ves}^0 is here observed. It can be considered as a residual influence of $\frac{\Delta S}{S_0}$, the more accurate C_0 values being those obtained with the largest magnetoliposomes: $C_0 = 0.02 \pm 0.005 \mu\text{m}^{-1}$.

We can evaluate for $R \approx 2 \mu\text{m}$ and $C_0 = 0.02 \mu\text{m}^{-1}$, $RC_0 \approx 4 \cdot 10^{-2}$ and $\frac{1}{2}K_b C_0^2 \approx 2 \cdot 10^{-11} \ll \tau$ (see Eq. (13)).

Let us comment on the physical origin of the spontaneous curvature we measure here. In [18], the determined C_0 values are 60 to 100 times larger, with magnetoliposomes similar to those used here. In that work an asymmetry of Debye length between the two sides of the membrane is arising from the different electrolyte compositions inside and outside the liposome. However, here the ionic strength is two orders of magnitude larger and the contribution of the nanoparticles to the Debye length is negligible with respect to that of the small ions. Thus here, there is no

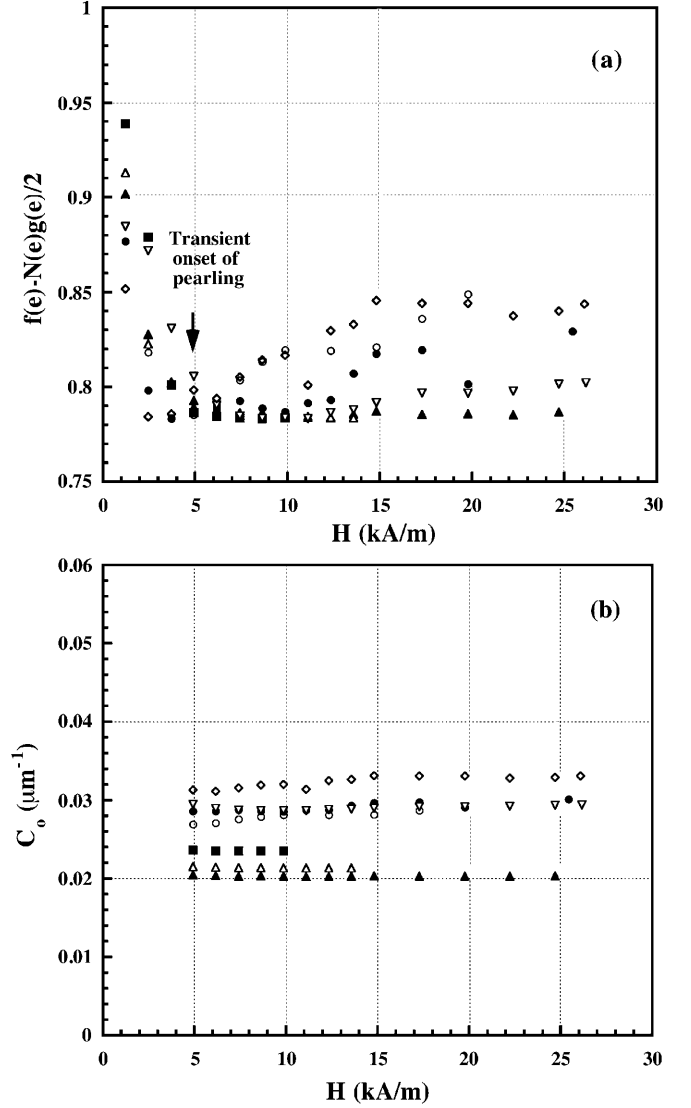


Fig. 9. a) Plot of $f(e) - \frac{N(e)g(e)}{2}$ as a function of H for the magnetoliposomes of initial radius $R_{\text{ves}}^0 \geq 40 \mu\text{m}$ (same symbols as in Fig. 6). b) Plot of the spontaneous curvature C_0 as a function of H in the pearling regime ($H > H_{\text{pearling}}$) for the magnetoliposomes of initial radius $R_{\text{ves}}^0 \geq 40 \mu\text{m}$ (same symbols as in Fig. 6). C_0 is deduced from equations (A.5) and (16): $C_0 = \frac{p_{\text{in}} - p_{\text{out}}}{\tau} = \frac{2}{R_{\text{ves}}^0} \left(f(e) - \frac{N(e)g(e)}{2} \right)$.

asymmetry coming from the electrostatic interaction between the nanoparticles and the membrane.

The steric contribution of non-adhesive particles to the spontaneous curvature is also negligible. Evaluating from [34] its order of magnitude gives here $C_0 \approx 10^{-4} \mu\text{m}^{-1}$ which is 100 times smaller than what we measure. Thus the C_0 value obtained here is not related to the presence of the nanoparticles inside the system. As is pointed out in [35], even for a symmetric solution across the membrane there is some asymmetry of the membrane left. Our $R_{\text{ves}}C_0$ value (of the order of 1.5) is quite close to that measured in [35] when there is no sugar asymmetry across the membrane.

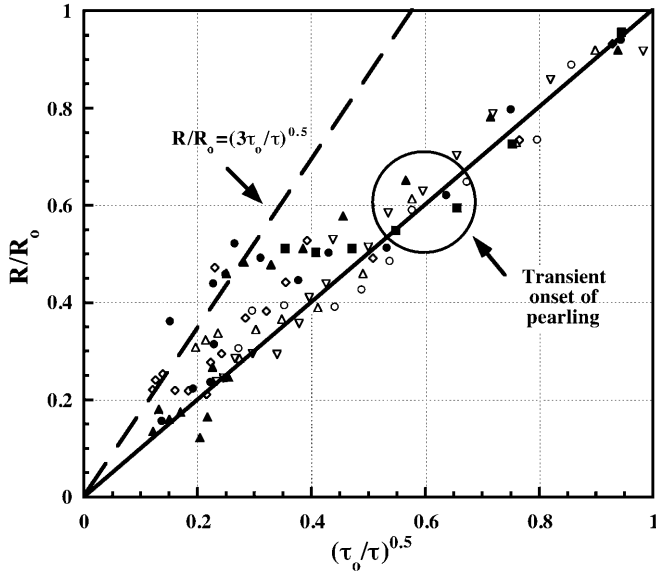


Fig. 10. Reduced representation of R/R_0 as a function of $(\tau_0/\tau)^{0.5}$ for the tube-connected magnetoliposomes (same symbols as in Fig. 6). The full line denotes the regime of evolution of a cylindrical tube with a uniform radius R . The dashed line corresponds to the theoretical onset of pearling given by equation (17).

4.3 Evolution of the radius of the tube and pearling instability

Figure 10 plots for different magnetoliposomes on the same graph the variations of $\frac{R}{R_0}$ as a function of $\sqrt{\frac{\tau_0}{\tau}}$. In the range of equilibrium of the cylindrical shape with a uniform circular section (that is for $\frac{R}{R_0}$ and $\sqrt{\frac{\tau_0}{\tau}}$ larger than 0.6 ± 0.1) the results more or less all superimpose together along the first bisectrix $\frac{R}{R_0} = \sqrt{\frac{\tau_0}{\tau}}$ expressing the decreasing of R as H increases. After the transient onset of pearling (that is for $\frac{R}{R_0}$ and $\sqrt{\frac{\tau_0}{\tau}}$ smaller than 0.6 ± 0.1) the experimental data spread between the two straight lines: i) $\frac{R}{R_0} = \sqrt{\frac{\tau_0}{\tau}}$ associated to the equilibrium of the cylindrical shape of uniform circular section and ii) $\frac{R}{R_0} = \sqrt{3\frac{\tau_0}{\tau}}$ associated to the theoretical threshold of pearling instability as deduced from equation (15) using our experimental determination of C_0 from Figure 9b. Indeed the parameter RC_0 is small ($RC_0 \leq 0.1$) and following equation (15) the pearling instability may develop only if the tension becomes larger than

$$\tau \geq \frac{3K_b}{2R^2}. \quad (17)$$

From expressions (7) and (8) it comes $\tau_0 = \frac{K_b}{2R_0^2}$ and $\tau_{\text{pearling}} = \frac{3K_b}{2R_{\text{pearling}}^2}$ thus the theoretical threshold of pearling corresponds to $\frac{R_{\text{pearling}}}{R_0} = \sqrt{3\frac{\tau_0}{\tau_{\text{pearling}}}}$. It is plotted as a dashed line in Figure 10. The experimental points spread between $\frac{R}{R_0} = \sqrt{\frac{\tau_0}{\tau}}$ and $\frac{R}{R_0} = \sqrt{3\frac{\tau_0}{\tau}}$, confornting the theoretical predictions [4–6,31]. However some dynamical

aspects seem to induce the pearling transition slightly below the theoretical threshold predicted statically in references [4–6,31]. Two arguments may support this point:

- the experimental wavelength λ of pearling is finite of the order of $20 \mu\text{m}$, for $R \approx 2 \mu\text{m}$, we obtain $kR \approx 0.6$, to be compared to the theoretical prediction of Figure 7: $kR = 0$ for $RC_0 \approx 0.1$;
- close to H_{pearling} we transiently observe some precursory deformations of the tube (see Fig. 5b) which frequently disappear and are much less developed than for larger fields (Fig. 5a).

Let us discuss now some dynamical aspects of the process that can influence the experimental threshold of pearling.

4.4 Dynamical aspects

There is a time delay between the response of the tube to reach its equilibrium radius and the quasi-immediate stress of the membrane produced by the field application. We can roughly evaluate those two characteristic times.

4.4.1 Characteristic time of diffusion of the tension along the membrane

The diffusion of the tension along the membrane of a tube of radius R is given [31] by

$$\frac{\partial \tau}{\partial t} = \frac{\kappa R}{4\eta} \frac{\partial^2 \tau}{\partial z^2},$$

κ being the compression modulus of the membrane and η the viscosity of water. It leads to a diffusion time along the tube

$$\theta_\tau = \frac{4\eta L^2}{\kappa R},$$

with $\kappa \approx 3 \cdot 10^{-2} \text{ Jm}^{-2}$, $\eta_{\text{water}} = 10^3 \text{ Pa s}$, $R = 2 \mu\text{m}$ and $L \approx 500 \mu\text{m}$ we obtain $\theta_\tau \approx 2 \cdot 10^{-2} \text{ s}$ which is much smaller than the experimental characteristic time of field increment ($\approx 30 \text{ s}$).

4.4.2 Characteristic time of relaxation of the tube radius

The diffusion time of the tube radius over a distance d is given by (see App. B)

$$\theta_R = \frac{d^2}{D_R} = \frac{2A\eta d^2}{5\tau R_i}.$$

For $d = \lambda = 20 \mu\text{m}$ the wavelength of pearling, $\eta_{\text{water}} = 10^{-3} \text{ Pa s}$, $R_i = 2 \mu\text{m}$ and varying τ from $3\tau_0$ at the transient onset of pearling up to its maximal value $100\tau_0$, we get a diffusion time θ_R ranging from 30 s down to 1 s. This characteristic time is of the same order of magnitude as the experimental characteristic time of field increment. From a dynamical point of view, the limiting

process for pearling instability is thus the relaxation of the tube radius and not the tension relaxation. In the pearling regime it may produce out-of-equilibrium situations. The hydrodynamical process of relaxation of the tube radius together with the dynamics of evolution of perturbations [31] determine the period of the selected unduloid.

4.5 Thermal fluctuations of the tube

We investigate here the tube properties through the measurements of the field-induced deformation of the magnetoliposome connected to the tube. Our experiments support the model of a magnetoliposome fed by an excess of membrane coming from the tube. This excess of tube membrane comes from a decrease of the tube radius due to an increase of the tension as the magnetic field increases. Nevertheless, another mechanism can be involved. The excess of membrane could also come from the vanishing of the thermal fluctuations of the tube membrane under field. A tentative estimate of the importance of this mechanism can be obtained with the simple model developed in Appendix C. It is clear that such a mechanism is largely insufficient to explain the large liposome deformations observed here.

5 Conclusion

We are dealing here with the shape stability of phospholipid tubes, a few microns in diameter. We present a new method to induce a pearling instability in such a phospholipid tube, this one being filled up with a magnetic liquid and connected to magnetoliposomes. An applied magnetic field modifies the stress of the membrane and if it exceeds a critical value it produces a peristaltic modulation of the tube. This method has several advantages over other methods. In particular, it provides a well-controlled tension source, it is reversible, there is no disruption of the membrane, by opposition to standard methods with optical tweezers.

We measure experimentally the under-field variations of the magnetoliposome eccentricity. Our theoretical model allows us to transform these experimental determinations in the variations of the tube radius R and of the pressure jump $p_{\text{in}} - p_{\text{out}}$, as a function of the applied tension.

Our model correctly describes the observed phenomena and provides us with determinations of membrane characteristics, namely in zero field its tension $\tau_0 \approx 10^{-8} \text{ J m}^{-2}$ and in the pearling regime its spontaneous curvature $C_0 \approx 0.02 \mu\text{m}^{-1}$.

In a first regime of applied fields, the phospholipid tube remains at equilibrium in a cylindrical conformation of uniform circular section and reduces its radius under the external solicitation. Under a large membrane tension, out-of-equilibrium situations are observed for the tube which develops a pearling instability because hydrodynamical processes prevent its radius reduction. In that

second regime the ratio $\frac{p_{\text{in}} - p_{\text{out}}}{\tau}$ is found to be a constant. The shape assumed by the tube is that of an unduloid of mean curvature equal to the spontaneous curvature of the membrane. This one can thus be determined here. The pearling observation roughly agrees with the theoretical predictions of references [4–6, 31], the experimental determination of the threshold being here penalized by the dynamics of relaxation of the tube radius.

We thank Olivier Sandre for useful exchanges and encouragements and Michel Lavergne who performed the electron micrographs in the SIARE of University Paris 6. We are also very grateful to the referees for their discerning and helpful comments.

Appendix A. Isolated liposomes in the general case of any eccentricity e

The deformation of a giant liposome due to tension follows a relation of elasticity that is particular to its entropic nature [23]:

$$\frac{(S_\tau - S_{\tau_0})}{S_{\tau_0}} \cong \frac{kT}{8\pi K_b} \ln \left(\frac{\tau}{\tau_0} \right). \quad (\text{A.1})$$

If we assimilate the elongated liposome to an ellipsoid of eccentricity e and of constant volume, the projected area writes:

$$S_\tau = S_{\tau_0} f(e) \quad (\text{A.2})$$

$$\text{with } f(e) = \left(\sqrt{1-e^2} + \frac{\arcsin(e)}{e} \right) \frac{1}{2(1-e^2)^{1/6}}.$$

For small deformations, it reduces to equation (2). Then equation (4) rewrites in the general case of any eccentricity e ,

$$\frac{(\mu - 1)^2}{16\pi} \frac{H^2 R_{\text{ves}}^0}{\tau} = \frac{g(e)}{2} \quad (\text{A.3})$$

$$\text{with } g(e) = \frac{\left(\frac{3-2e^2}{e^2} - (3-4e^2) \frac{\arcsin(e)}{e^3(1-e^2)^{1/2}} \right)}{(1-e^2)^{2/3} \left(\frac{(3-e^2)}{e^5} \ln \left(\frac{1+e}{1-e} \right) - \frac{6}{e^4} \right)}.$$

As well, equation (5) rewrites, in the general case of any eccentricity e ,

$$p_{\text{in}} - p_{\text{out}} = \frac{2\tau}{R_{\text{ves}}^0} f(e) - \frac{(\mu - 1)^2}{8\pi} N(e) H^2 = \frac{2\tau}{R_{\text{ves}}^0} \left(f(e) - \frac{1}{2} N(e) g(e) \right), \quad (\text{A.4})$$

where the demagnetizing factor of the ellipsoid is given by

$$N(e) = \frac{(1-e^2)}{2e^3} \left(\ln \left(\frac{1+e}{1-e} \right) - 2e \right). \quad (\text{A.5})$$

Equation (A.3) then simplifies in

$$\frac{45kT}{32\pi K_b} \left(\frac{\tau_0}{\tau}\right)^2 \left(\frac{H}{H^*}\right)^4 = \frac{g(e)^2}{4}. \quad (\text{A.6})$$

For small eccentricities, expression (A.6) reduces to equation (6).

Appendix B. Characteristic time of relaxation of the tube radius

It is natural to suppose that the time response of the tube radius relaxation to a small increment $\delta\tau$ of its tension is governed by the hydrodynamic flow of the liquid inside the tube, the more so for a tube with peristaltic deformations. In the framework of the lubrication approximation, with a tube of initial radius R_i aligned along the z -axis, it comes

$$R(z, t) = R_i + \delta R(z, t),$$

$$\frac{\partial(\pi R^2(z, t))}{\partial t} + \frac{\partial Q}{\partial z} = 0 \quad (\text{B.1})$$

with $Q = -\frac{5\pi}{24\eta} R_i^4 \frac{\partial p_{\text{in}}}{\partial z}$, where η is the viscosity of the fluid inside the tube and p_{in} its pressure. The increment δp_{in} of pressure inside the tube is linked to δR and $\delta\tau$ by relation (3) with $\mathbf{k}_G = 0$, $\Delta_B \mathbf{H} = 0$ and $\mathbf{H} = -\frac{1}{2R}$ through

$$\delta(\Delta p) = \delta p_{\text{in}} = \delta \left(\frac{\tau}{R} - \frac{K_b}{2R^3} \right) = -\tau \frac{\delta R}{R_i^2} + \frac{\delta\tau}{R_i} + \frac{3K_b}{2R_i^4} \delta R.$$

Using the equilibrium condition

$$\tau = \frac{K_b}{2R_i^2} \quad \text{gives} \quad \delta p_{\text{in}} = \frac{1}{R_i} \delta\tau + \frac{2\tau}{R_i^2} \delta R$$

and thus, neglecting the term in $\frac{\partial\delta\tau}{\partial z}$ with respect to that in $\frac{\partial\delta R}{\partial z}$:

$$\frac{\partial p_{\text{in}}}{\partial z} = \frac{\partial\delta p_{\text{in}}}{\partial z} \approx \frac{2\tau}{R_i^2} \frac{\partial\delta R}{\partial z}.$$

Equation (B.1) then writes

$$\frac{\partial(\delta R)}{\partial t} = D_R \frac{\partial^2(\delta R)}{\partial z^2} \quad \text{with} \quad D_R = \frac{5\tau R_i}{24\eta}$$

and leads to the diffusion time of the tube radius over a distance d :

$$\theta_R = \frac{d^2}{D_R} = \frac{24\eta d^2}{5\tau R_i}.$$

Appendix C. Flattening of the thermal fluctuations of the tube

The excess of membrane of the liposome connected to a tube could come from the vanishing of the thermal fluctuations of the tube membrane under field. A simple estimate of the importance of such a mechanism is derived here. In this model the tube of mean radius R_0 is viewed like a string with a tension $2\pi R_0\tau$ and a curvature elasticity $2\pi R_0 K_b$, as in reference [4]:

$$E = 2\pi R_0 \int \left[\tau + \frac{K_b}{2} \left(\frac{\partial^2 \vec{u}}{\partial z^2} \right)^2 \right] \cdot \sqrt{1 + \left(\frac{d\vec{u}}{dz} \right)^2} dz,$$

\vec{u} being the displacement of the membrane perpendicular to its main axis Oz .

A decomposition in Fourier series

$$\vec{u} = \frac{1}{L} \sum_k \vec{u}_k \exp(ikz)$$

gives for the energy variation of the tube with length L

$$\Delta E = \frac{\pi R_0}{L} \sum_k [\tau k^2 + K_b k^4] \cdot |\vec{u}_k|^2.$$

The theorem of energy equipartition allows to write the fluctuations of the tube length as $\delta l = \langle L \rangle - L = L \frac{kT}{2\pi^2 R_0} \int \frac{k^2 dk}{\tau k^2 + K_b k^4}$, the fluctuations along \vec{Ox} and \vec{Oy} axes being independent. If we assume that the maximal and minimal values of the wave number k_{max} and k_{min} are such as $k_{\text{min}} \ll \sqrt{\frac{\tau}{K_b}} \ll k_{\text{max}}$, we can evaluate the area of the tube δS absorbed in the thermal undulations:

$$\delta S = 2\pi R_0 \delta l = 2\pi R_0 L \frac{kT}{4\pi K_b \sqrt{2}} \sqrt{\frac{\tau_0}{\tau}}. \quad (\text{C.1})$$

In equation (C.1), the slope of δS versus $\sqrt{\frac{\tau_0}{\tau}}$ is smaller by a factor $\frac{kT}{4\sqrt{2}\pi K_b} \approx 3 \cdot 10^{-3}$ than in our model and in the experiment. The amount of lipid absorbed by the liposome because of the flattening of the thermal fluctuations of the tube is here negligible. In the presence of an applied magnetic field the dominant effect is the diminution of the tube radius under the increase of the tension of the membrane.

References

1. B.J. Marsh, D.N. Mastronarde, K.F. Buttler, K.E. Howell, J.R. McIntosh, Proc. Natl. Acad. Sci. USA, **98**, 2399 (2001).
2. R.S. Polishchuk, E.V. Polishchuk, P. Marra, S. Alberti, R. Buccione, A. Luini, A.A. Mironov, J. Cell Biol. **148**, 45 (2000).
3. R. Bar-Ziv, T. Tlusty, E. Moses, S.-A. Safran, A. Bershadsky, Proc. Natl. Acad. Sci. USA **96**, 10140 (1999).

4. R. Bar-Ziv, E. Moses, *Phys. Rev. Lett.* **73**, 1392 (1994).
5. P. Nelson, T. Powers, U. Seifert, *Phys. Rev. Lett.* **74**, 3384 (1995).
6. R. Bar-Ziv, T. Tlusty, E. Moses, *Phys. Rev. Lett.* **79**, 1158 (1997).
7. J.Z. Young, *Nature* **154**, 521 (1944).
8. S. Ochs, R. Pourmand, R.A. Jersild, *Neuroscience* **70**, 1081 (1996).
9. H. Ringsdorf, B. Schlarb, J. Veenzmer, *Angew. Chem. Int. Ed. Engl.* **27**, 113 (1988).
10. V. Frette, I. Tsafrir, M.-A. Guedeau-Boudeville, L. Jullien, D. Kandel, J. Stavans, *Phys. Rev. Lett.* **83**, 2465 (1999).
11. I. Tsafrir, D. Sagi, M.-A. Guedeau-Boudeville, V. Frette, D. Kandel, J. Stavans, *Phys. Rev. Lett.* **86**, 1138 (2001).
12. M.-A. Guedeau-Boudeville, A.-L. Bernard, J.-C. Bradley, A. Singh, L. Jullien in *Giant Vesicles*, edited by P.-L. Luisi, P. Walde (John Wiley & Sons, Chichester, 2000) pp. 341-349.
13. R. Massart, *IEEE Trans. Magn.* **17**, 1247 (1981).
14. J.-C. Bacri, R. Perzynski, D. Salin, V. Cabuil, R. Massart, *J. Magn. & Magn. Mater.* **85**, 77 (1990).
15. F. Pincet, S. Cribier, E. Perez, *Eur. Phys. J. B* **11**, 127 (1999).
16. H. Egawa, K. Furusawa, *Langmuir* **15**, 1660 (1999).
17. L. Xu, Döberheiner H.-G., in *Giant Vesicles*, edited by P.-L. Luisi, P. Walde (John Wiley & Sons, Chichester, 2000) pp. 181-184.
18. O. Sandre, C. Ménager, J. Prost, V. Cabuil, J.-C. Bacri, A. Cebers, *Phys. Rev. E* **62**, 3865 (2000).
19. J.-C. Bacri, V. Cabuil, A. Cebers, C. Ménager, R. Perzynski, *Europhys. Lett.* **33**, 235 (1996).
20. W. Helfrich, *Z. Naturforsch.* **28c**, 693 (1973).
21. W. Helfrich, R. Servuss, *Nuovo Cimento D*, **3**, 137 (1984).
22. Lord Rayleigh, *Scientific Papers* **1**, 361, 379 (1964).
23. E. Evans, W. Rawicz, *Phys. Rev. Lett.* **64**, 2094 (1990).
24. J.-C. Bacri, D. Salin, *J. Phys. (Paris)* **43**, L-649 (1982).
25. M.B. Schneider, J.T. Jenkins, W.W. Webb, *J. Phys. (Paris)* **45**, 1457 (1984) (see also the earlier paper by J.T. Jenkins, *J. Math. Biol.* **4**, 149 (1977)).
26. Ou-Yang Zhong-Can, W. Helfrich, *Phys. Rev. A* **39**, 5280 (1989).
27. A. Cebers, *Magn. Gidrodin.* **1**, 25 (1985) (in Russian).
28. E. Blums, A. Cebers, M.M. Maiorov, *Magnetic Fluids* (de Gruyter, New York, 1997).
29. For equilibrium shapes, energetics and virial method give identical results.
30. G. Bossis, A. Cebers, *Magn. Gidrodin.* **33**, 75 (1997) (in English).
31. R.E. Goldstein, P. Nelson, T. Powers, U. Seifert, *J. Phys. II* **6**, 767 (1996).
32. C. Delaunay, *J. Math. Pure Appl. Ser.* **1(6)**, 309 (1841); J. Eells, *Math. Intell.* **9**, 53 (1987).
33. H. Naito, M. Okuda, Ou-Yang Zhong-Can, *Phys. Rev. Lett.* **74**, 4345 (1995).
34. R. Lipowsky, H.G. Döbereiner, *Europhys. Lett.* **43**, 219 (1998).
35. H.G. Döbereiner, O. Shelchow, R. Lipowsky, *Eur. Biophys. J.* **28**, 174 (1999).